# Characterization of the Extent of Internal Motions in Oligosaccharides†

T. J. Rutherford, J. Partridge,‡ C. T. Weller, and S. W. Homans*

*Department of Biochemistry, University of Dundee, Dundee DD1 4HN, Scotland, U.K.*

*Received July 13, 1993; Revised Manuscript Received September 15, 1993*®

ABSTRACT: A detailed investigation has been undertaken on the extent and nature of torsional fluctuations about the glycosidic linkage of the model disaccharide Man$\alpha$1-3Man$\alpha$1-OMe. In particular, we sought to determine whether the three nuclear Overhauser effects and the two long-range heteronuclear $^3J_{CH}$ spin coupling constants measurable across the glycosidic linkage were consistent with a single conformation or multiple conformations about that linkage. Within experimental error, we have found that these five parameters can be interpreted in terms of a single, rigid geometry. Alternatively, the data are also consistent with a model in which the glycosidic torsional angles exhibit significant but restricted fluctuations about the global minimum energy conformation. Evidence from restrained molecular dynamics simulations both *in vacuo* and with explicit inclusion of solvent water and from $^{13}C$ relaxation measurements upon an oligomannose glycan in covalent association with protein suggests that the latter model is the most accurate representation of the conformational behavior of oligosaccharides in solution.

There is currently much debate regarding the extent and nature of internal motions in oligosaccharides. Early investigations of the solution conformations of oligosaccharides using nuclear Overhauser effect and spin coupling constant measurements together with conformational energy calculations led to the conclusion that the majority of glycosidic linkages in N-linked glycans were essentially fixed in a single conformation, resulting in an overall conformation for the molecule which was relatively "rigid" (Lemieux et al., 1980; Thogersen et al., 1982; Homans et al., 1982; Brisson & Carver, 1983a,b,c; Sabesan et al., 1984; Paulsen et al., 1986). However, more detailed analyses have led to the alternative hypothesis that significant conformational averaging takes place in solution and that conformational models based on the assumption of a single conformation about glycosidic linkages are "virtual" conformations (Cumming & Carver, 1987). In this regard, a variety of conformational studies on oligosaccharides using NMR[1] have been described in recent years by several groups (Cumming et al., 1987; Homans et al., 1987a,b,c; Scarsdale et al., 1988; Breg et al., 1989; Imberty et al., 1989; Poppe et al., 1990; Yan & Bush, 1990; Cagas & Bush, 1990; Peters et al., 1990; Edge et al., 1990; Homans, 1990; Tran & Brady, 1990; Wormald et al., 1991; Homans & Forster, 1992), and the conclusions from these studies regarding the overall conformational properties of oligosaccharides vary, some describing very restricted motion about glycosidic linkages and others concluding that a variety of conformations exist about such linkages. While it is possible that the extent of torsional oscillation about glycosidic linkages may depend on the precise oligosaccharide studied, there remain inconsistencies with currently published observations. For example, in early work, experimental measurements were in excellent agreement with conformational models of a variety of N-linked glycans assuming a single, rigid conformation about most glycosidic linkages (Brisson & Carver, 1983a,b,c), and yet these same data can apparently also be interpreted in terms of significant motional averaging (Cumming & Carver, 1987).

In principle, the extent of torsional oscillations about glycosidic linkages in oligosaccharides can be determined with use of molecular dynamics simulations (Brady, 1986, 1987; Homans et al., 1987c; Yan & Bush, 1990; Homans, 1990; Homans & Forster, 1992). However, the parametrization of molecular mechanical force fields for oligosaccharides is not as well developed as that for proteins, and free dynamics simulations of oligosaccharides are open to question regarding their accuracy, particularly in regions of conformational space divorced from the global minimum. One means by which such simulations can be verified in part is to back-calculate experimentally measurable parameters (NOEs and spin coupling constants) from the simulations. In recent studies on the trisaccharide Man$\alpha$1-3Man$\beta$1-4GlcNAc (Homans, 1990) and on the pentasaccharide Gal$\beta$1-4(Fuc$\alpha$1-3)-GlcNAc$\beta$1-3Gal$\beta$1-4Glc (Homans & Forster, 1992), we used this approach to compare experimentally measured nuclear Overhauser effects or rotating-frame Overhauser effects (ROEs) with those derived theoretically from free molecular dynamics simulations of the same oligosaccharides with explicit inclusion of solvent water. In each case we found restricted torsional oscillations about glycosidic linkages, and the theoretically determined Overhauser effects were in good agreement with experimental values. However, despite these favorable comparisons, a residual criticism of this work may be that the dynamics simulations are not of sufficient length. By virtue of computational time requirements, these are restricted to nanoseconds at most and might not adequately span the conformational space which is actually "seen" by the molecule over the time scale of measurement of Overhauser effects, i.e., tens to hundreds of milliseconds. If this criticism proves valid, then again it raises the paradox by which experimental data are consistent with both "rigid" and "flexible" geometry about glycosidic linkages.

A possible reason for this duality is the dearth of experimental constraints about many glycosidic linkages in oligo-

† This work was funded by the LINK Biotransformations program of the Science and Engineering Research Council and The Department of Trade and Industry and by Celltech, Glaxo, ICI, and The Wellcome Foundation. S.W.H. is a Lister Institute Centenary Research Fellow.

‡ Present address: Department of Biotechnology, Royal College, George St., University of Strathclyde, Glasgow, U.K.

® Abstract published in *Advance ACS Abstracts,* November 1, 1993.

[1] Abbreviations: NMR, nuclear magnetic resonance; NOE, nuclear Overhauser effect; NOESY, two-dimensional nuclear Overhauser effect spectroscopy; ROESY, two-dimensional rotating-frame Overhauser effect spectroscopy.

0006-2960/93/0432-12715$04.00/0 

saccharides. For example, often only one NOE is measurable across the glycosidic linkage, and it is easy to visualize in these circumstances how such a constraint is consistent with both conformational models. In the present study, we attempt to overcome this limitation by means of an extensive study on a model disaccharide within which a significant number of experimental constraints can be measured accurately. The chosen compound is Man$\alpha$1-3Man$\alpha$1-OMe, within which three Overhauser effects can be observed across the glycosidic linkage, together with two long-range heteronuclear $^3J_{CH}$ couplings, providing information on the glycosidic torsional angles. Our approach is to determine whether these five constraints are consistent with a single conformation about the glycosidic linkage of the disaccharide or whether it is necessary to invoke conformational averaging in order to predict accurately the observed experimental data. These data are then assessed in light of $^{13}C$ relaxation time measurements for a glycan chain containing the Man$\alpha$1-3Man unit in covalent association with the parent protein.

## MATERIALS AND METHODS

NMR measurements on Man$\alpha$1-3Man$\alpha$1-OMe were performed at 300 K on a sample prepared by dissolution of 5 mg in 0.5 mL 99.96% $D_2O$. Bovine pancreatic ribonuclease B was purchased from Sigma (catalog no. R 5875) and was further purified by affinity chromatography on ConA–Sepharose (Sigma). The glycan component was digested to a single species (Man$\alpha$1-6(Man$\alpha$1-3)Man$\alpha$1-6Man$\alpha$1-3)-Man$\beta$1-4GlcNAc$\beta$1-4GlcNAc) with jack bean $\alpha$-mannosidase (Oxford Glycosystems), and the glycoprotein was purified by gel permeation chromatography. The sample for NMR investigations was prepared by dissolution of 30 mg of glycoprotein in 0.5 mL of 99.96% deuterium oxide (Aldrich).

Homonuclear $^1H$ nuclear Overhauser effect measurements (Macura & Ernst, 1980) were performed in the conventional manner with a variety of mixing time values to plot the buildup time of the NOE in the case of Man$\alpha$1-3Man$\alpha$-1-OMe or with a fixed mixing time of 200 ms in the case of ribonuclease B, and magnetization derived from coherence transfer was suppressed by random variation of the mixing time $\tau_m$. Long-range heteronuclear $^3J_{CH}$ coupling constants were obtained as described by Norwood et al. (1990) by use of conventional two-dimensional, multiple-bond, heteronuclear, single-quantum correlation experiments, which after zero-filling and two-dimensional Fourier transformation gave rise to a two-dimensional spectrum with a final digital resolution of 0.2 Hz/point in the $F_2$ dimension. Long-range $^3J_{CH}$ coupling constants were measured directly from antiphase multiplets in the $F_2$ dimension of the spectrum.

Two-dimensional, inverse-detected $^{13}C$ $T_1$ and $T_2$ measurements were recorded at 125 MHz using the pulse sequences described by Kay et al. (1989), with a spectral width of 6000 Hz, 256 $t_1$ increments, and 128 transients per increment. In the case of the inverse $T_1$ experiment, five spectra were acquired with relaxation delays of 10 $\mu$s and 50, 100, 150, and 250 ms. The delay between 180° pulses in the inverse $T_2$ experiment was 1.4 ms, resulting in a pulse train whose duty cycle was just below the maximum permitted by the transmitter protection circuits. Five experiments were acquired with relaxation delays of 4.8, 11.2, 22.4, 39.2, and 56 ms. After two-dimensional Fourier transformation, data were apodized by application of exponential functions corresponding to a line broadening of 10 Hz in the $t_2$ dimension and 20 Hz in the $t_1$ dimension. Crosspeak volumes were obtained using the integration routine of conventional Bruker UXNMR software, following third-order polynomial base-line correction in both dimensions. Analysis of relaxation data in terms of the Lipari and Szabo model (Lipari & Szabo, 1982a,b) was achieved with use of a modified version of a program kindly provided by Dr. Mark Forster.

Restrained simulated annealing and restrained molecular dynamics simulations were performed both *in vacuo* and with explicit inclusion of solvent water under periodic boundary conditions according to previously described protocols (Homans & Forster, 1992). In simulations with explicit inclusion of water, the disaccharide was solvated in a box 25 Å × 25 Å × 25 Å. Nuclear Overhauser effect distance restraints were classified as strong, medium, or weak and were applied as biharmonic restraints with lower and upper bounds of 1.8–2.7, 1.8–3.3, and 1.8–5.0 Å, respectively. Dihedral angle constraints were obtained from measured $^3J_{CH}$ values, which were converted to angles by use of the appropriate Karplus relationship (Tvaroska et al., 1989). Full relaxation matrix calculations were performed with the aid of the program NOEMOL (Forster et al., 1989).

In all molecular mechanical calculations, the force field used was that described previously (Homans, 1990), but since we were intent on defining the extent of torsional fluctuations by experimental means as far as possible, all torsional terms describing the glycosidic linkage, including the *exo*-anomeric effect, were set to 0. Certain investigations described below involved a series of starting configurations for the disaccharide with pseudorandom values of $\varphi$ and $\psi$, and these were created by running a dynamics simulation for the disaccharide *in vacuo* at 750 K, followed by rapid quenching to 300 K at 10-ps intervals. In this manner, a series of geometries is created in regions of conformational space with relatively low energy, thus avoiding to a large extent problems which arise during minimization of starting structures which are of very high energy.

## CONVENTIONS

The torsional angles $\varphi$, $\psi$, and $\omega$ are analogous to $\varphi_H$, $\psi_H$, and $\omega_H$ in IUPAC convention and are defined as H1–C1–O1–CX, C1–O1–CX–HX, and H5–C5–C6–O6, where CX and HX are aglyconic atoms.

We have adopted the nomenclature of Vliegenthart et al. (1983) for identifying each monosaccharide residue in the digested glycan (Man$\alpha$1-6(Man$\alpha$1-3)Man$\alpha$1-6(Man$\alpha$1-3)-Man$\beta$1-4GlcNAc$\beta$1-4GlcNAc) of ribonuclease B, i.e.,

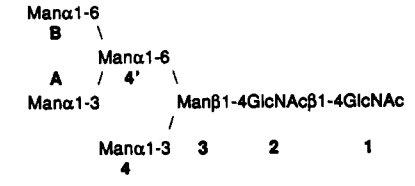


## RESULTS AND DISCUSSION

Measured NOE values at mixing times of 750 ms and 1.5 s and measured $^3J_{CH}$ values for the two glycosidic torsion angles in the disaccharide are shown in Table I. All NOE values were positive at these mixing times.

In an initial series of investigations, we sought to discover whether these five experimental restraints were consistent with a single structure for the disaccharide. A collection of nine geometries was created with pseudorandom values of $\varphi$ and $\psi$ (see Materials and Methods), and each geometry was subjected to a restrained simulated annealing calculation in

Table I: Measured NOE and $^3J_{CH}$ Values for Manα-1-3Manα-1-OMe

| spin pair | absolute NOE (%)[a] | relative NOE[b] |
|---|---|---|
| | $\tau_m$ = 750 ms | |
| Manα1-H1–Manα1-H2 | 2.4 | 1.00 |
| Manα1-H1–3Manα-H2 | jd[c] | 0.0 |
| Manα1-H1–3Manα-H3 | 4.0 | 1.64 |
| Manα1-H5–3Manα-H2 | 1.3 | 0.54 |
| | $\tau_m$ = 1.5 s | |
| Manα1-H1–Manα1-H2 | 3.2 | 1.00 |
| Manα1-H1–3Manα-H2 | jd[c] | 0.0 |
| Manα1-H1–3Manα-H3 | 4.5 | 1.4 |
| Manα1-H5–3Manα-H2 | 1.3 | 0.4 |

| dihedral angle | $^3J_{CH}$ |
|---|---|
| H1–C1–O1–C3 ($\varphi$) | 4.00 ± 0.2 |
| C1–O1–C3–H3 ($\psi$) | 5.1 ± 0.2 |

[a] Estimated maximum error in NOE measurements is ±20%. [b] Relative NOEs calculated with respect to the intraresidue NOE between Manα1-H1 and Manα1-H2. [c] jd, just detectable.

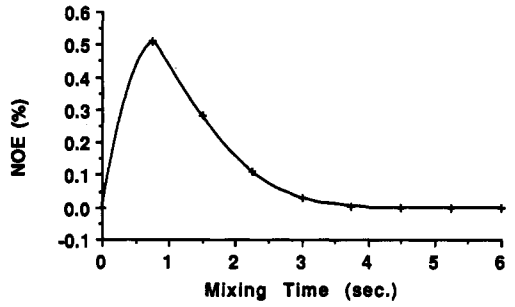


FIGURE 1: Time dependence of the NOE between Manα1-H1 and 3Manα-H2 in Manα1-3Manα1-OMe, computed with a full relaxation matrix analysis assuming a spectrometer frequency of 500.13 MHz and an overall correlation time $\tau_c$ of 0.15 ns (Brisson & Carver, 1983a). The glycosidic torsion angles were adjusted ($\varphi$ = 0°, $\psi$ = 17°) such that Manα1-H1 and 3Manα1-H3 were at the distance of closest approach (2.07 Å), with the distance between Manα1-H1 and 3Manα1-H2 equal to 3 Å. For further details, see text.

an attempt to locate the global minimum energy configuration for the disaccharide.

In a first calculation, only the three NOE restraints were used, and these were classified empirically as weak, medium, or strong, in complete analogy to the procedures adopted for the structural analyses of proteins (Wuethrich, 1986). In the case of the weak NOE corresponding to the connectivity Manα1-H1 to 3Manα1-OMe-H2, the choice of distance bounds is, in principle, complicated by two conflicting NOE pathways between these two protons—apart from the direct pathway, there is the possibility of a competing negative NOE via a three-spin effect involving 3Manα1-OMe-H3, which might result in a small NOE even when Manα1-H1–3Manα1-OMe-H2 are relatively close. However, at all times we were careful to measure NOEs within the initial rate approximation, under which conditions the three-spin effect does not contribute significantly, as evidenced by calculations on a series of geometries of the disaccharide using a full-relaxation matrix analysis. The rate of buildup of the relevant NOE is shown in Figure 1 for a geometry in which Manα1-H1 and 3Manα1-OMe-H3 are at the distance of closest approach (where the three-spin effect is maximal) and in which the distance between Manα1-H1 and 3Manα1-OMe-H2 is 3.0 Å. Since the NOE between Manα1-H1 and 3Manα1-OMe-H2 is ~0.5% at the mixing time (750 ms) used to obtain experimental NOE values (Table I), and since the calculated value based on the spin pair approximation is ~0.7% (which would be just above the noise level), from these data we reasoned that the influence

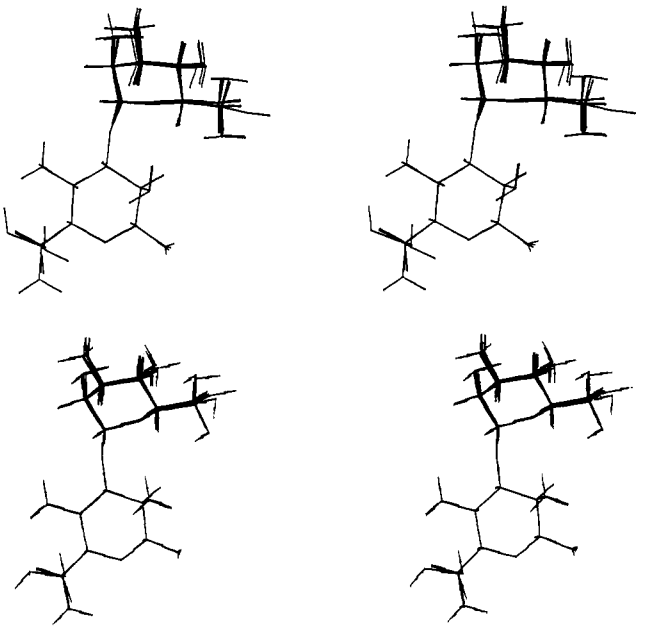

FIGURE 2: (Top) Family of structures derived from nine pseudo-random starting geometries, using the restrained simulated annealing strategy described in the text, and with the three NOE restraints given in Table II. (Bottom) As above, but with the addition of the two dihedral angle restraints shown in Table II.

of the three-spin effect was not large, and the relevant distance bound was thus defined as "weak". The NOEs between Manα1-H1 and 3Manα1-OMe-H3 and between Manα1-H5 and 3Manα1-OMe-H2 were each defined as "strong". By use of these constraints, a family of six structures was found as a result of the simulated annealing strategy, each with a similar geometry at $\varphi,\psi \approx -47°,+20°$ and no constraint violations (Figure 2a). The remaining three structures had skewed ring geometries due to the imperfect nature of the simulated annealing strategy and were discarded.

A second calculation was performed in an identical manner to the first but with the inclusion of the two dihedral angle constraints. The derivation of upper and lower angle bounds for the dihedral constraints is not straightforward, since a measured $^3J_{CH}$ could correspond to a single, fixed geometry or could, in principle, correspond to some average over 360°. However, the purpose of this second calculation was to assess whether the experimentally derived dihedral angles were also consistent with the single family of structures derived from the first calculation. The upper and lower bounds for the angular constraints were therefore taken as the measured value minus or plus the error in measurement, respectively, allowing for the fact that both positive and negative values of the angle would give the same measured $^3J_{CH}$. By use of these constraints, a family of seven structures was found as a result of the simulated annealing strategy, each with a similar geometry at $\varphi,\psi \approx -36°,+18°$ and with constraint violations which were small (Figure 2b and Table II). As in the first calculation, the remaining two structures either possessed constraint violations or had skewed ring geometries due to the imperfect nature of the simulated annealing strategy and were discarded.

From the family of structures obtained in the second calculation, it is possible to compute theoretical NOE and $J$ values for comparison with experiment (Table III), and it is seen that a single family of structures is acceptably consistent with all five experimentally measured parameters, and hence it is not necessary to invoke conformational averaging about the glycosidic linkage to account for the experimental data.

Table II: Geometries and Final Energies Resulting from Restrained Annealing of Nine Pseudorandom Geometries of Manα1-3Manα1-OMe[a]

| structure | φ (deg)[b] | ψ (deg)[b] | interatomic distances[c] NOE$_1$ | NOE$_2$ | NOE$_3$ | total energy (kcal/mol) |
|---|---|---|---|---|---|---|
| 1 | −36.33 (0.04) | +17.08 | 2.16 | 2.77 | 3.51 | −0.20 |
| 2[d] | −29.02 | −1.31 | 2.14 | 4.92 | 3.79 | 5.77 |
| 3 | −36.92 (0.07) | +18.01 | 2.18 | 2.72 | 3.50 | −0.24 |
| 4 | −35.22 (0.01) | +18.5 | 2.17 | 2.85 | 3.48 | 0.06 |
| 5[e] | +37.56 (0.1) | −1.58 | 2.24 | 5.24 (0.6) | 3.20 (0.89) | 0.93 |
| 6 | −35.3 (0.01) | +19.0 (0.01) | 2.18 | 2.84 | 3.47 | 0.35 |
| 7 | −36.67 (0.05) | +18.11 | 2.18 | 2.73 | 3.50 | −0.18 |
| 8 | −36.71 (0.06) | +18.49 | 2.19 | 2.70 | 3.49 | 0.51 |
| 9 | −35.34 (0.01) | +18.6 | 2.17 | 2.82 | 3.48 | 0.53 |

[a] Constraint violations greater than 0.01 kcal mol$^{-1}$ are shown in parentheses. [b] Lower ($\varphi_l$,$\psi_l$) and upper ($\varphi_u$,$\psi_u$) bounds for angular restraints and restraint force constants ($k$) as follows: φ(H1–C1–O1–C3); $\varphi_l$ = −34.0°, $\varphi_u$ = +34.0°, $k$ = 25 kcal mol$^{-1}$ Å$^{-2}$; ψ(C1–O1–C3–H3), $\psi_l$ = −18.0°, $\psi_u$ = +18.0°, $k$ = 25 kcal mol$^{-1}$ Å$^{-2}$. [c] NOEs, their lower ($r_l$) and upper ($r_u$) distance bounds and restraint force constants ($k$) are as follows: NOE$_1$, Manα1-H1–3Manα-H3, $r_l$ = 1.8 Å, $r_u$ = 2.7 Å, $k$ = 10 kcal mol$^{-1}$ Å$^{-2}$; NOE$_2$, Manα1-H5–Manα1-H2, $r_l$ = 1.8 Å, $r_u$ = 2.7 Å, $k$ = 10 kcal mol$^{-1}$ Å$^{-2}$; NOE$_3$, Manα1-H1–3Manα-H2, $r_l$ = 1.8 Å, $r_u$ = 5.0 Å, $k$ = 10 kcal mol$^{-1}$ Å$^{-2}$. [d] Skewed chair geometry of Manα1 unit. [e] Geometry of Manα1 unit inverted to Manβ.

Table III: Comparison of Experimental NOE and $^3J_{CH}$ Values with Theoretical Values Derived from (top) Single Geometry Corresponding to Structure 3 in Table II and (bottom) Motional Model Derived from the 500-ps *in Vacuo* Molecular Dynamics Simulation of Figure 3

| spin pair/dihedral angle | theoretical parameters NOE ⟨$r^{-6}$⟩ | NOE ⟨Tropp⟩ | $^3J_{CH}$ | measured parameters[a] NOE | $^3J_{CH}$ |
|---|---|---|---|---|---|
| Manα1-H1–3Manα-H3 | 2.29 | NA[b] | | 1.64 ± 0.32 | |
| Manα1-H5–3Manα-H2 | 0.61 | NA[b] | | 0.54 ± 0.10 | |
| Manα1-H1–3Manα-H2 | 0.13 | NA[b] | | jd[c] | |
| H1–C1–O1–C3 | | | 3.66 | | 4.00 ± 0.2 |
| C1–O1–C3–H3 | | | 5.09 | | 5.1 ± 0.2 |
| Manα1-H1–3Manα-H3 | 1.82 | 1.98 | | 1.64 ± 0.32 | |
| Manα1-H5–3Manα-H2 | 0.77 | 0.61 | | 0.54 ± 0.10 | |
| Manα1-H1–3Manα-H2 | 0.04 | 0.09 | | jd[c] | |
| H1–C1–O1–C3 | | | 3.44 | | 4.00 ± 0.2 |
| C1–O1–C3–H3 | | | 4.59 | | 5.1 ± 0.2 |

[a] NOE values reported are relative NOEs calculated with respect to the intraresidue NOE between Manα1-H1 and Manα1-H2. The estimated error in these measurements is ±20%. $^3J_{CH}$ values reported are in hertz, with error values equal to the digital resolution in the HSQC experiment from which they were measured. However, as noted in the text, the actual error may be significantly greater. [b] NA, not applicable. [c] jd, just detectable.

In particular, the theoretical relative NOE of 0.13 translates to an absolute NOE of 0.3%, which would be just detectable, in agreement with the experimental value. Of note is the fact that the predicted values of φ and ψ are similar to those measured previously using entirely different protocols (Homans et al., 1987c), and it is particularly interesting that the value of φ for the single family of structures in Table II is on the order of that predicted by the *exo*-anomeric effect, yet we have not included an *exo*-anomeric term in the current computational strategy.

To determine whether the experimental data were also consistent with a model involving torsional fluctuations about φ and ψ in the disaccharide, we intended to explore the conformational space available about φ and ψ using an *in vacuo* molecular dynamics simulation. We reasoned that if this simulation bore a resemblance to the true extent of torsional oscillations about φ and ψ in solution, then a back-calculation of the three NOE and two $^3J_{CH}$ values from the simulation should be in good agreement with experiment. However, from such simulations of up to 1 ns in length and under various conditions either in the absence or in the presence of an *exo*-anomeric term, we were unable to obtain satisfactory agreement between experimental and simulated NOE and $^3J_{CH}$ values (data not shown). It should be emphasized that the inability to simulate experimental data was not simply a result of simulations of insufficient length, since certain regions of conformational space were sampled for substantial periods during the simulations, behavior which could be excluded on the basis of the measured NOEs and $^3J_{CH}$ values. Similar efforts by others in the simulation of experimental NMR data from grid-search calculations, where φ,ψ conformational space is by definition sampled in full, have also met with limited success (Imberty et al., 1989). While a possible interpretation of these data is that there is no model involving torsional motions for the disaccharide which is consistent with experimental data, it is our contention that current molecular mechanical force fields for oligosaccharides, including that developed in this laboratory (Homans, 1990) and used in the present study, are of insufficient accuracy in regions divorced from the global minium to simulate such a model should it exist. This is not surprising in view of the fact that small errors in simulated average distances will be magnified to the sixth power in computation of the relative NOE. We therefore chose to compute a *restrained* MD simulation *in vacuo*, using the three NOE restraints with distance bounds described above. While such a simulation may not reveal the true dynamic nature of the disaccharide, we reasoned that it would reveal whether at least one motional model was in existence which was consistent with all the data. In this calculation, the angular constraints were not included, since it is impossible to define exactly the angular bounds to which they correspond. The regions of conformational space mapped during the last 500 ps of this 510-ps simulation are plotted in Figure 3. Average NOE and $^3J_{CH}$ values were thus calculated from the last 500 ps of the simulation, with the NOEs calculated as a simple $r^{-6}$ average and a more complex average appropriate for internal motions which are fast compared with overall tumbling ("Tropp-average"), as described previously (Homans & Forster, 1992). Strictly, neither of these formulations is appropriate for the type of motion implied in Figure 3, since while the internal motions are clearly fast with respect to the overall motion, these motions are stongly coupled in a simple disaccharide. Nevertheless, the computed NOE values are in good agreement with experiment (Table III). In particular, it should again be noted that the computed NOE between Manα1-H1 and 3Manα1-OMe-H2 (relative NOE at 4% or 9% depending on the model) translates to an absolute NOE of 0.1% or 0.22%, which approaches the limit of detection in agreement with the experimental measurement. In larger oligosaccharides where the NOE is large and negative, a

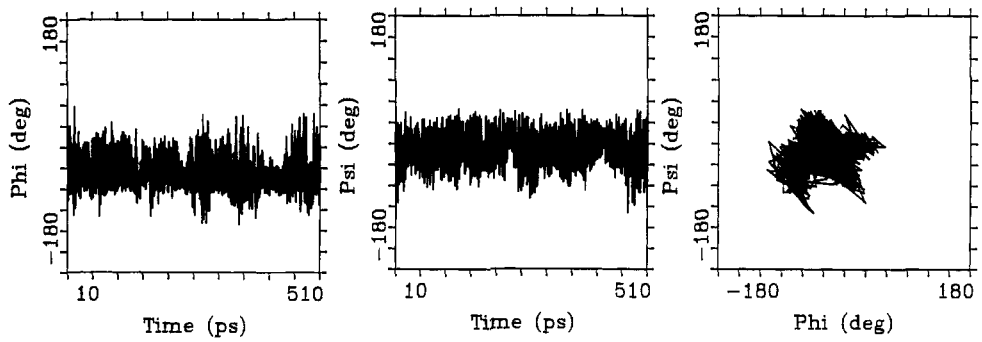


FIGURE 3: Plots of $\varphi$ (left), $\psi$ (center), and $\varphi$ vs $\psi$ (right) for the 500-ps restrained molecular dynamics simulation *in vacuo* of Man$\alpha$1-3Man$\alpha$1-OMe, with the three NOE restraints and distance bounds given in Table II.

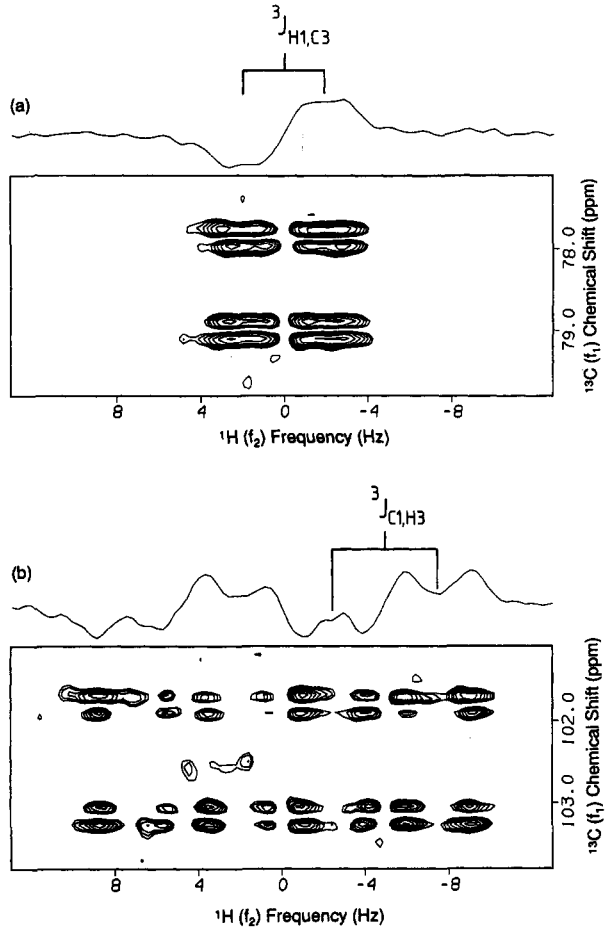


FIGURE 4: Crosspeaks derived from the HSQC spectrum of Man$\alpha$1-3Man$\alpha$1-OMe and their projections. (a) Crosspeak correlating Man$\alpha$1-H1 with 3Man$\alpha$-C3; (b) crosspeak correlating Man$\alpha$1-C1 with 3Man$\alpha$-H3. The $^3J_{CH}$ coupling constants are extracted from antiphase splittings as shown.

significant negative NOE or positive ROE is easily measurable between Man$\alpha$1-H1 and 3Man$\alpha$1-OMe-H2 in the Man$\alpha$1-3Man fragment (Homans et al., 1987a; T. J. Rutherford et al., University of Dundee, unpublished data). The computed $^3J_{CH}$ values agree less well with experiment. However, although the theoretical error in their measurement corresponds to the digital resolution of the HSQC experiment (±0.2 Hz), in practice there is a significant subjective uncertainty when manually measuring long-range couplings in these experiments, as is apparent from the projections of the relevant crosspeaks from the HSQC spectrum (Figure 4), and hence the true error is difficult to quantify but is significantly larger than this. We would consider agreement to within approximately ±0.5 Hz, to be satisfactory.

The computation of experimental parameters from a restrained MD simulation such as that described above is open to criticism in the sense that it should be possible at least to extract the experimental data which were applied in the form of distance constraints. However, the back-calculated relative NOEs could, in principle, adopt a very wide range of values without violating the distance constraint (e.g., that between Man$\alpha$1-H1 and 3Man$\alpha$1-H3 could range between ~0.6 and 7.2), yet these compute to values close to those determined experimentally. Furthermore, two additional lines of evidence suggest that the conformational space explored in Figure 3 might be realistic. First, the values of $\varphi$ and $\psi$ which are sampled in Figure 3 correspond closely to the minimum energy regions of grid-search calculations for the disaccharide (Imberty et al., 1989), and second, the back-calculated $^3J_{CH}$ values are in reasonable agreement with experiment, yet no angular constraints are applied during the simulation.

In a final series of calculations, we sought to examine the influence of solvent water on the dynamics of the disaccharide by inclusion of explicit water molecules in a restrained molecular dynamics simulation. In previous work, such simulations led to restricted torsional oscillations about glycosidic linkages in comparison with *in vacuo* simulations, and in general a single conformation was observed over time scales extending to several hundred picoseconds (Homans, 1990; Homans & Forster, 1992). However, as discussed above, on the NMR time scale, multiple conformational states cannot be excluded. To address this point, a series of nine initial starting geometries were constructed for the disaccharide in the presence of solvent water with use of a quenching procedure, as described in the Materials and Methods section. This procedure ensures that each starting geometry is in a pseudorandom local minimum rather than some arbitrary conformation with randomly chosen values of $\varphi$ and $\psi$ which may possess a very high initial energy. Each of these structures was then subjected to 150 ps of restrained molecular dynamics simulation using the NOE constraints defined above, and the conformational space mapped during the final 100 ps of each simulation is shown in Figure 5. A total of four discrete conformational states are observed, and three of these fall within the bounds of the conformational space mapped in the *in vacuo* simulation (Figure 3). These data, therefore, suggest that the conformational space mapped in simulations with explicit inclusion of solvent water may be similar to that observed in *in vacuo* simulations but that the probability of conformational transitions is much reduced in the former. An interesting feature of the data in Figure 5 is the presence of a quasistable conformation at $\varphi = 30°, \psi = -150°$ (simulations 4 and 7), corresponding to a shallow minimum in grid-search calculations (Imberty et al., 1989), which is not observed in the simulation *in vacuo* (Figure 3). This conformation is not

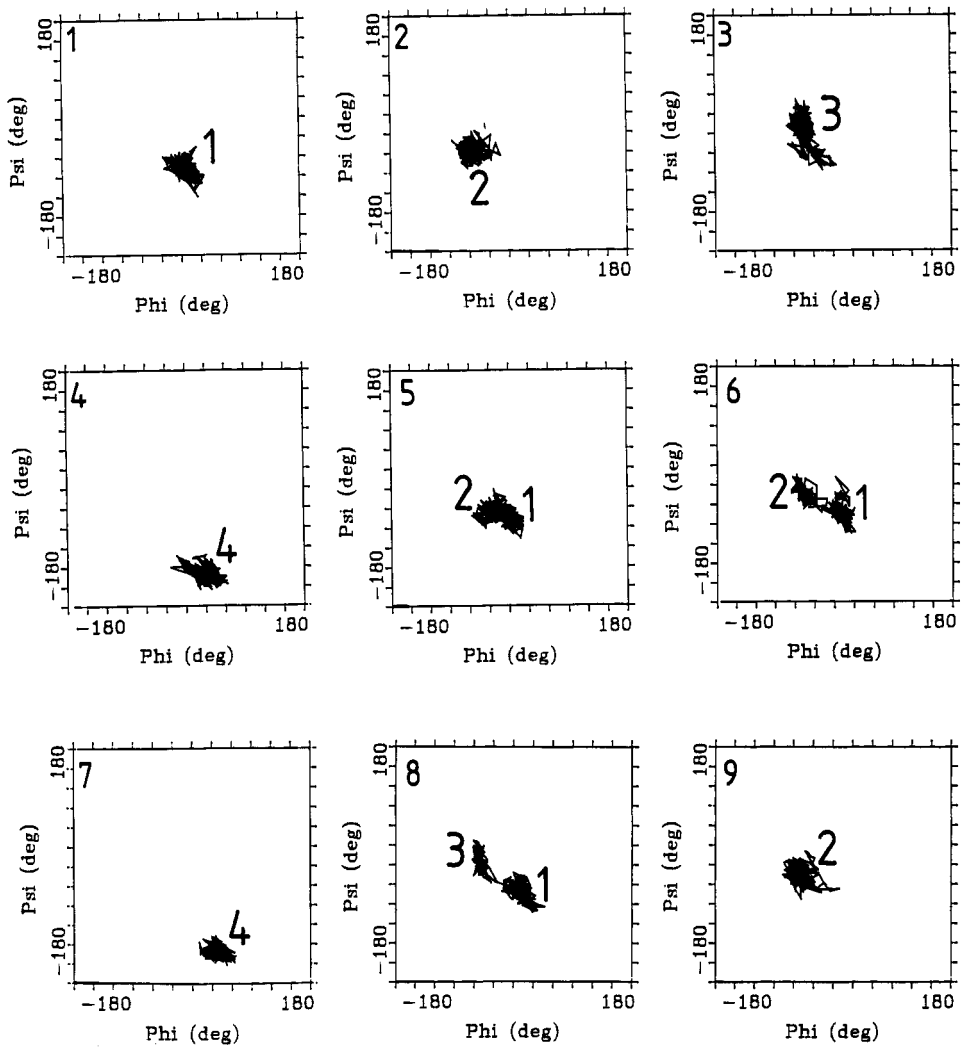


FIGURE 5: Plots of $\varphi$ vs $\psi$ over the last 100 ps of a 150-ps restrained molecular dynamics simulation with explicit inclusion of solvent water and with the NOE restraints and distance bounds defined in Table II. Each of these simulations (labeled 1–9 in the top left hand corner of each panel) derives from an initial conformation obtained by a dynamic quenching procedure (see methods section). A total of four discrete conformational states are mapped during these simulations, labeled 1–4 in each panel.

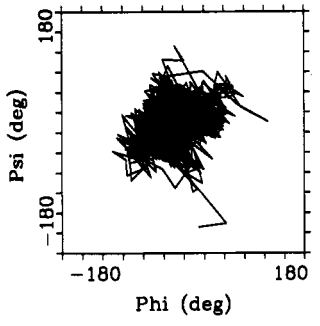


FIGURE 6: (a) Plot of $\varphi$ vs $\psi$ for the unrestrained molecular dynamics simulation *in vacuo* of Man$\alpha$1-3Man$\alpha$1-OMe, with an initial geometry which was located at the quasistable conformation seen in panels 4 and 7 of Figure 7 (i.e., with $\varphi$, $\psi$ = 30°,–150°). The full 510-ps trajectory is plotted to illustrate the rapid exit from the starting conformation.

observed if the *in vacuo* simulation is repeated with an initial geometry located at this quasistable conformation, even in the complete absence of NOE constraints (Figure 6). The simulation exits rapidly from this minimum. In any event, this conformation cannot be populated significantly, since the computed values of the NOEs between Man$\alpha$1-H1 and 3Man$\alpha$1-OMe-H3 and between Man$\alpha$1-H5 and 3Man$\alpha$1-OMe-H2 are ~10% of their experimentally measured values (Table IV). Therefore, while this conformation is clearly stable over 100 ps, it must be short-lived in comparison with the spin–lattice relaxation time (tens of milliseconds). In fact, none of the simulations in Figure 5 yields computed average NOE or $^3J_{CH}$ values which are in good agreement with

Table IV: Computed Average NOE and $^3J_{CH}$ Values for Man$\alpha$1-3Man$\alpha$1-OMe Derived from the Nine 100-ps Molecular Dynamics Simulations with Explicit Inclusion of Solvent Water Shown in Figure 5

| | NOE $\langle r^{-6}\rangle^b$ | | | $^3J_{CH}{}^c$ | |
|---|---|---|---|---|---|
| simulation[a] | 1 | 2 | 3 | 1 | 2 |
| 1 | 1.56 | 0.05 | 0.04 | 5.2 | 2.7 |
| 2 | 0.70 | 1.00 | 0.03 | 1.8 | 4.2 |
| 3 | 1.74 | 1.13 | 0.09 | 2.8 | 4.9 |
| 4 | 0.16 | 0.03 | 0.03 | 4.2 | 3.5 |
| 5 | 1.48 | 0.07 | 0.04 | 4.9 | 3.0 |
| 6 | 1.83 | 0.20 | 0.05 | 4.7 | 3.3 |
| 7 | 0.16 | 0.04 | 0.03 | 3.2 | 3.6 |
| 8 | 1.88 | 0.35 | 0.06 | 4.5 | 3.5 |
| 9 | 1.16 | 1.13 | 0.05 | 2.6 | 4.9 |

[a] Each simulation refers to the analogous panel in Figure 5. [b] NOE values reported are relative NOEs calculated with respect to the intraresidue NOE between Man$\alpha$1-H1 and Man$\alpha$1-H2 and are as follows: 1, Man$\alpha$1-H1–3Man$\alpha$-H3; 2, Man$\alpha$1-H5–3Man$\alpha$-H2; and 3, Man$\alpha$1-H1–3Man$\alpha$-H2. [c] $^3J_{CH}$ values reported are in hertz and correspond with the following glycosidic dihedral angles: 1, H1–C1–O1–C3; 2, C1–O1–C3–H3.

experiment (Table IV). (Note here that a simple $r^{-6}$ average calculation is appropriate since the rate of interconversion of conformations is slow relative to overall tumbling). We attribute this to the poor mapping of conformational space over the time scales of the simulations, coupled with the fact that the NOE and $^3J_{CH}$ values are very sensitive to small variations in $\varphi$ and $\psi$. For example, simulations 2 and 5 appear superficially to map similar regions of conformational space, yet the computed NOE and $^3J_{CH}$ values are very different.

The results of the above MD simulations suggest indirectly that the "motional" model of oligosaccharide dynamics is correct. To confirm this, we attempted to obtain direct evidence for the presence of such motions by NMR spin relaxation time measurements. In probing oligosaccharide dynamics in solution, measurement of $^{13}C$ relaxation times is the method of choice, since the relaxation is dominated to a good approximation by the directly bonded proton, which therefore simplifies subsequent analysis of the data. Several investigations have focused on $^{13}C$ relaxation time measurements of isolated oligosaccharides in free solution (McCain & Markley, 1986; Kadkhodaei et al., 1991; Cagas & Bush, 1992), and the dynamic information avilable under these circumstances is limited because each monosaccharide residue essentially moves independently and the relaxation parameters become relatively insensitive to differential mobility within the molecule (Levy et al., 1978). In addition, for small oligosaccharide fragments such as disaccharides and trisaccharides, and to a certain extent for larger oligosaccharides, the internal motions cannot be decoupled from overall rotational tumbling, and the interpretation of relaxation data in terms of internal correlation times and generalized order parameters (Lipari & Szabo, 1982a,b) becomes impossible. To overcome this difficulty, we undertook proton-detected $^{13}C$ relaxation measurements of the oligomannose glycan of ribonuclease B, in association with the parent protein. The oligomannose glycan contains two Man$\alpha$1-3Man moieties, and hence these measurements should confirm the predictions based on the model disaccharide above and at the same time provide important information on the remaining glycosidic linkages in this glycan. By undertaking the relaxation measurements on the intact glycoprotein, these measurements should be more sensitive to the much faster internal motions of the glycan, since the latter is effectively "tethered" at its reducing end. Ribonuclease B has been the subject of previous $^{13}C$ relaxation studies at 67.9 MHz. (Berman et al., 1981) but since conventional, low-sensitivity $^{13}C$-detected methods were employed, the data were of insufficient accuracy to allow the details of oligosaccharide dynamics to be quantified.

Plots of ln(crosspeak intensity) vs relaxation delay for the proton-detected $^{13}C$ $T_1$ and $T_2$ experiments are shown in Figure 7. Not shown are the relaxation data for GlcNAc 2 C-1, since these were obscured by solvent water, for GlcNAc 1 C-1, which was too weak to integrate, and for Man B C-2 and Man 3 C-2, for which reliable integrals could not be obtained due to proximity with strong protein resonances at $\omega1,\omega2$ = 72.0,3.8 ppm and 67.0,4.2 ppm, respectively. In addition, the H-1/C-1 and H-2/C-2 resonances of Man 4 and Man A exactly overlapped, and hence their individual relaxation terms could not be separated. In all cases it was necessary to maintain a relatively short maximum relaxation delay, since the signal-to-noise ratio of the spectra at long delay times was too poor to be of value. From each of the plots in Figure 7, $T_1$ and $T_2$ were extracted by least-squares fitting, and these values are given in Table V. In an attempt to quantify the measured $T_1$ and $T_2$ values for each resonance in terms of intramolecular motion of each residue in the oligosaccharide, these values were then fitted to the formalism of Lipari and Szabo (1982a,b) for the extraction of generalized order parameters ($S^2$) and internal correlation times ($\tau_e$). To utilize this formalism, it is necessary to assume that the overall tumbling of the glycoprotein is isotropic, which is a good approximation for a globular protein such as ribonuclease, even bearing a relatively bulky N-linked glycan. Since the signal-to-noise ratio of either the $T_1$ or the $T_2$ spectrum was insufficient to allow relaxation data to be derived for the protein, the overall correlation time $\tau_m$ necessary for the extraction of $S^2$ and $\tau_e$ was estimated from the Stokes–Einstein relation to be $\sim$4.3 $\times$ $10^{-9}$ s, and this value, which is similar to that derived previously [(8 $\pm$ 2) $\times$ $10^{-9}$ s, Berman et al. (1981)] was used in all calculations. The fitted $T_1$ and $T_2$ values together with $S^2$ and $\tau_e$ values are shown in Table V. It is seen that good fits were obtained for all resonances (sum-of-squares < 0.000 13) with the exception of 3C-1, for which a relatively poor fit was obtained (sum-of-squares $\approx$ 0.20). We attribute this to the relavively poor quality of the measured relaxation data for this resonance which, by virtue of its relatively rapid decay, results in signals which approach the noise at longer delays, especially in $T_2$ measurements.

Table V: Experimental and Fitted $T_1$ and $T_2$ Values,[a] Together with Calculated Values of $S^2$ and $\tau_e$ for Each of the Five Mannose Residues of the Glycan of Ribonuclease B

| | $T_1$ (s) | | $T_2$ (s) | | $S^2$ | | $\tau_e$ |
|---|---|---|---|---|---|---|---|
| resonance | exptl | fitted | exptl | fitted | measd | calcd | ($\times 10^9$ s) |
| 1 C-1[b] | <0.23 | | <0.06 | | | 0.72 | |
| 2 C-1 | nd[c] | | nd[c] | | | 0.63 | |
| 3 C-1 | 0.23 | 0.31 | 0.06 | 0.08 | 0.47 | 0.52 | 2.021 |
| 4/A C-1 | 0.39 | 0.39 | 0.24 | 0.24 | 0.11 | 0.28/0.14 | 0.198 |
| 4/A C-2 | 0.41 | 0.40 | 0.18 | 0.18 | 0.20 | nd[c] | 0.186 |
| 4′ C-1 | 0.41 | 0.41 | 0.11 | 0.11 | 0.46 | 0.57 | 0.210 |
| 4′ C-2 | 0.35 | 0.35 | 0.11 | 0.11 | 0.41 | nd[c] | 0.320 |
| B C-1 | 0.42 | 0.43 | 0.14 | 0.14 | 0.32 | 0.24 | 0.175 |

[a] For all calculations, an overall rotational correlation time of 4.3 $\times$ $10^{-9}$ was utilized, assuming isotropic reorientation of the protein backbone. For each entry in the table, the sum of squares resulting from the fitting procedure was $\leq$0.000 13, except for Man 3 C-1, which was 0.24. [b] Relaxation times for this resonance were too rapid to measure. [c] nd, not determined.

From the data in Table V it is immediately seen that there exists a significant variation in $S^2$ and $\tau_e$ values for each residue in the oligosaccharide. In particular, Man 3 exhibits the largest values of $S^2$ and $\tau_e$, which indicates that Man 3 has considerably less mobility than other residues in the glycan, and exhibits a rate of internal motion which is considerably slower. Since the proton and carbon chemical shifts for all of the residues considered here are identical to those observed in the free glycan (Berman et al., 1981), we consider it unlikely that this "restricted" motion derives from direct steric interference from side-chain atoms of the protein. Rather, we argue that this derives from the inherent proximity of Man 3 to the slowly tumbling protein. Indeed, the relatively low $S^2$ value ($\sim$0.49) and the high $\tau_e$ value (0.21 $\times$ $10^{-8}$, which approaches $\tau_m$) are consistent with significant but restricted torsional flexibility about glycosidic linkages between this residue and the protein. It follows from this argument that if similar torsional flexibility exists about the other glycosidic linkages, then $S^2$ and $\tau_e$ should both decrease for residues more distal from the protein. It is seen from Table V that this is generally the case. All residues distal from Man 3 are seen to possess values of $\tau_e$ which are 1 order of magnitude smaller than that of Man 3, and $S^2$ for Man B appears to be significantly smaller than that of Man 4′, which would be consistent with greater freedom of motion

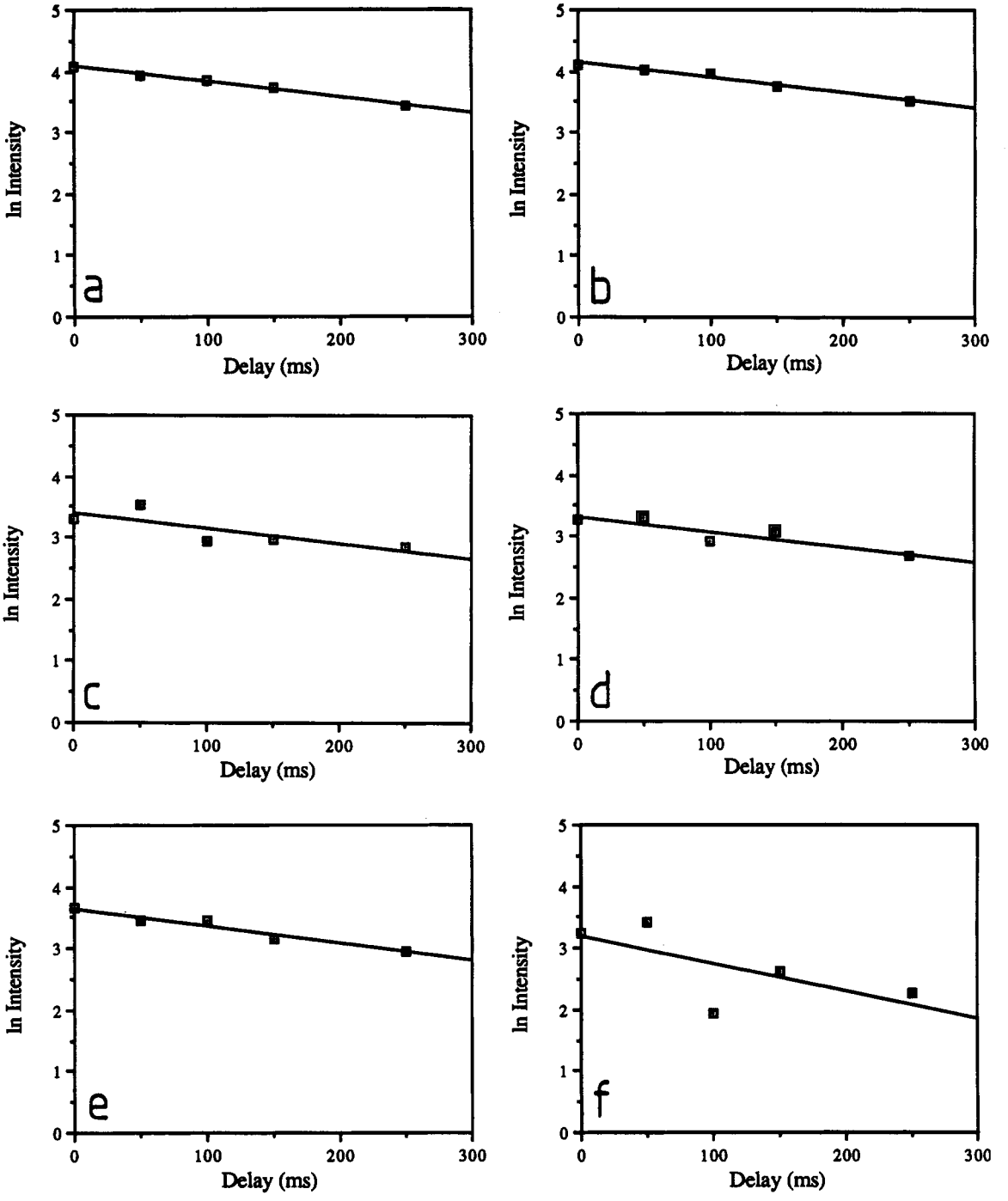


FIGURE 7: Plots of ln(crosspeak intensity) vs relaxation delay derived from "inverse-detected" $T_1$ and $T_2$ measurements on ribonuclease B. Each panel corresponds with the following: $T_1$ data, (a) 4/A C-1, (b) 4/A C-2, (c) B C-1, (d) 4′ C-1, (e) 4′ C-2, (f) 3 C-1; $T_2$ data, (g) 4/A C-1, (h) 4/A C-2, (i) B C-1, (j) 4′ C-1, (k) 4′ C-2, (l) 3 C-1. Not shown are relaxation data for resonances 1 C-1 and 2 C-1, B C-2 and 3 C-2, for which reliable integrals could not be obtained. Solid lines indicate least-squares fits of the data.

resulting from the additional, "flexible" $\alpha$1-6 linkage (Brisson & Carver, 1983a,b,c; Homans et al., 1987a,b,c; Cumming & Carver, 1987). An apparent discrepancy is seen for Man 4, which would be anticipated to possess less motional freedom than Man B or Man 4′ due to the lower torsional flexibility of the Man$\alpha$1-3Man$\beta$ linkage in comparison with the Man$\alpha$1-6Man$\beta$ linkage. A possible reason for this discrepancy lies in the fact that the relaxation parameters for Man A and Man 4 are inseparable due to exact resonance overlap. Mobility of Man A will be reflected in relatively long $T_1$ and $T_2$ values, which might obscure the underlying, more rapid decay of magnetization from Man 4, and hence the reported $S^2$ value would primarily reflect the motion of A.

As an aid to understanding further the apparently anomalous mobility of residue 4, an attempt was made to model the dynamics of the oligosaccharide with use of a 60-ps *in vacuo* restrained molecular dynamics simulation of ribonuclease B. Initial attempts were hampered by the strong Coulombic interactions between the protein and the oligosaccharide *in vacuo*, even with a dielectric constant of 80.0. Since it was unrealistic to model the glycoprotein with explicit inclusion of solvent water on grounds of available CPU time, the problem was overcome by setting the partial charges on the protein (but not on the oligosaccharide) to 0. We justify this approximation by noting that the sole purpose of the simulation was to examine the dynamics of the oligosaccharide only, and

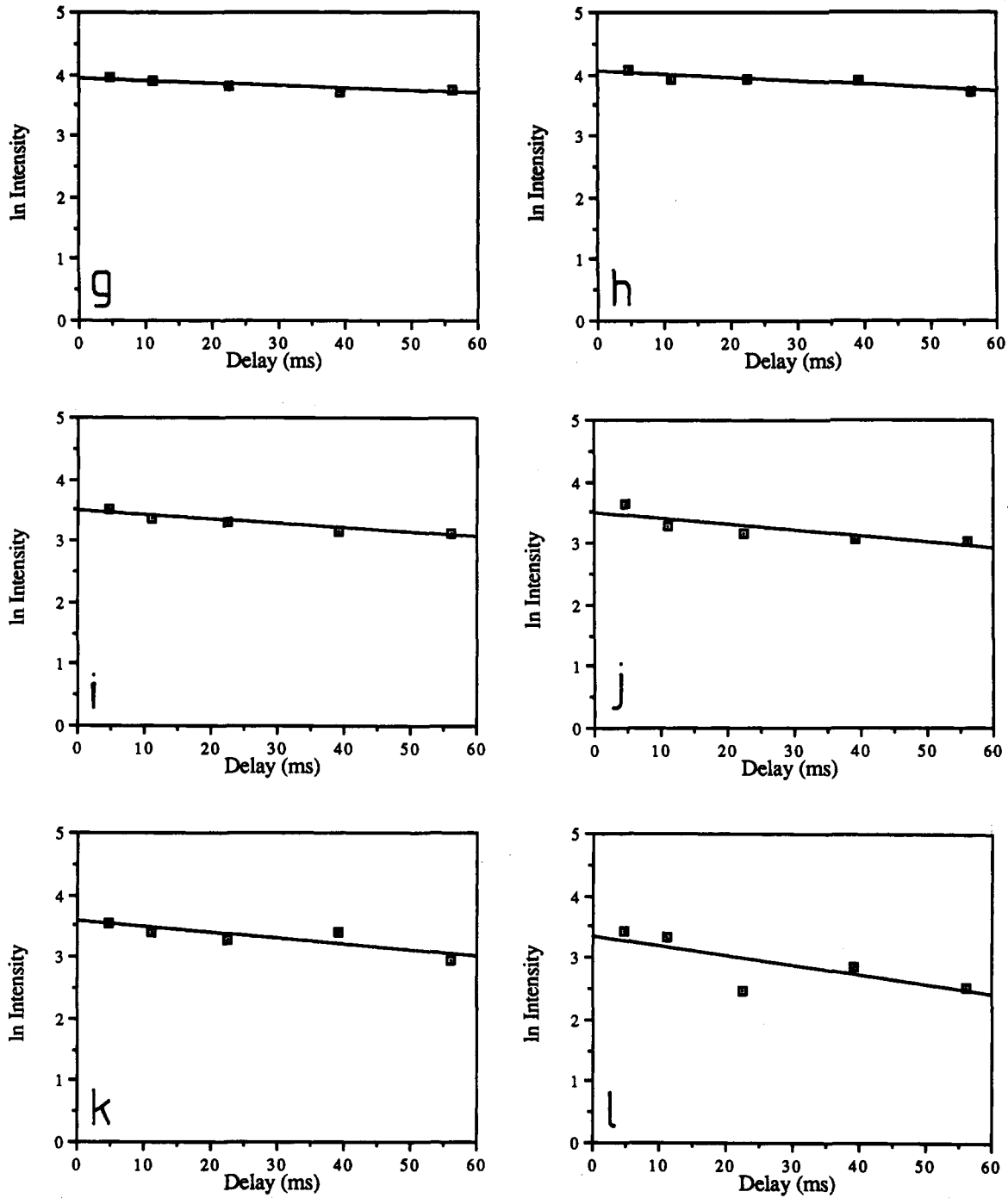


FIGURE 7: (Continued)

in view of the essential identities of the proton and carbon shifts between the free and protein-bound oligosaccharide, it is highly unlikely that any interactions exist between the oligosaccharide and the protein which would constrain the former in any way. To compare the extent of torsional variation ($S^2$ values) of each residue derived experimentally (above) with that predicted from the simulation, autocorrelation functions were computed for the C-1–H-1 bond vector of each monosaccharide residue and are shown in Figure 8. In each case, a rapid initial decay due to fast internal motions is followed by a plateau which decays slowly to 0 at a rate governed by slow overall tumbling of the macromolecule. This phenomenon is entirely analogous to that observed for the side chains of proteins, and, in common with previous studies (Levy et al., 1981), we take the value of the correlation function at the plateau as a measure of $S^2$, and these values are given in Table V. It is appreciated that a simulation of 60 ps in length, which was constrained by available CPU time, is barely adequate as a measure of $S^2$ on account of the measured $\tau_e$ values for the glycan. However, it should be remembered that the experimentally derived $\tau_e$ values are relevant to internal dynamics in the presence of solvent, whereas an *in vacuo* molecular dynamics simulation was performed here, under which conditions the rates of internal motion are accelerated by at least 1 order of magnitude (Homans, 1990). Nevertheless, in the case of certain residues, notably 4′, A, and B, an initial plateau is followed by a second, more rapid decay at ~30 ps which derives from conformational transitions about $\omega$ at both $\alpha$1-6 glycosidic linkages and which barely reaches a second plateau before termination of the simulation. Thus the reported $S^2$ values for residues 4′, A, and B are the maximum predicted values.

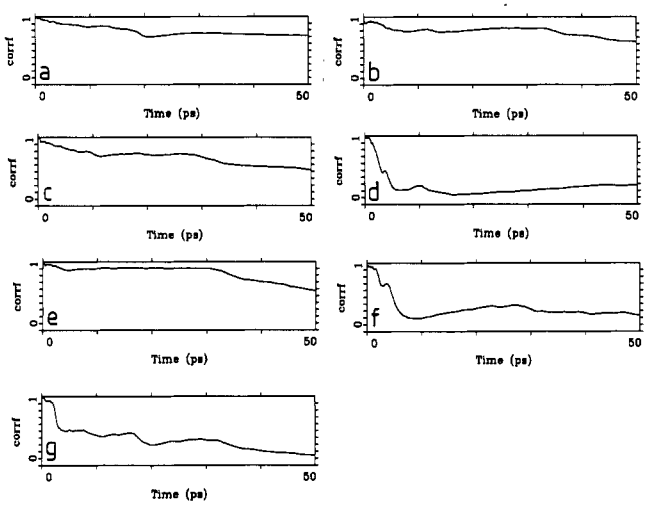


FIGURE 8: Autocorrelation functions (corrf) plotted over the final 50 ps of the restrained molecular dynamics simulation *in vacuo* for ribonuclease B. Each panel refers to the C-1–H-1 bond vector of each monosaccharide residue of the glycan in ribonuclease B as follows: (a) GlcNAc 1, (b) GlcNAc 2, (c) Man 3, (d) Man 4, (e) Man 4′, (f) Man A, (g) Man B.

Exact correspondence between experimental and theoretical $S^2$ values is not anticipated, since the experimental values are strictly *generalized* order parameters (Lipari & Szabo 1982a,b). Nevertheless, inspection of Table V shows that the experimental and theoretical values of $S^2$ are in reasonable agreement.

## CONCLUSIONS

The purpose of this study was to determine whether the three NOE and two $^3J_{CH}$ values measurable across the glycosidic linkage of Man$\alpha$1-3Man$\alpha$1-OMe are compatible with a single conformation about the glycosidic linkage or whether it is necessary to invoke conformational averaging to explain the observed parameters. As seen in Table III, reasonable agreement is obtainable between theoretical and experimental parameters when a single, rigid geometry is assumed. In fact, only the theoretical NOE between Man$\alpha$1-H1 and 3Man$\alpha$-H3 deviates significantly from the experimental value. However, a motional model can also be devised whereby the measured NOE values are in excellent agreement with theoretical values. The experimental values of $^3J_{CH}$ agree less well with theoretical values than those assuming rigid geometry, but, as mentioned above, the actual error in the experimental values of $^3J_{CH}$ may be significantly greater than indicated. Despite the relatively large number of experimental constraints, it is impossible within experimental error to distinguish between "rigid" and "motional" models of oligosaccharide solution behavior on the basis of NOE and $^3J_{CH}$ measurements, at least for the model disaccharide studied here. To distinguish these models, it was necessary to resort to $^{13}C$ relaxation time measurements of an oligosaccharide in covalent association with protein, from which it is apparent that the "motional" model is the correct interpretation of the solution behavior of the Man$\alpha$1-3Man glycosidic linkage.

## REFERENCES


Berman, E., Walters, D. E., & Allerhand, A. (1981) *J. Biol. Chem. 256*, 3853.

Brady, J. W. (1986) *J. Am. Chem. Soc. 108*, 8153.

Brady, J. W. (1987) *Carbohydr. Res. 165*, 306.

Breg, J., Kroon-Batenburg, L. M. J., Strecker, G., Montreuil, J., & Vliegenthart, J. F. G. (1989) *Eur. J. Biochem. 178*, 727.

Brisson, J.-R., & Carver, J. P. (1983a) *Biochemistry 22*, 1362.

Brisson, J.-R., & Carver, J. P. (1983b) *Biochemistry 22*, 3671.

Brisson, J.-R., & Carver, J. P. (1983c) *Biochemistry 22*, 3680.

Cagas, P., & Bush, C. A. (1990) *Biopolymers 30*, 1123.

Cagas, P., & Bush, C. A. (1992) *Biopolymers 32*, 277.

Cumming, D. A., & Carver, J. P. (1987) *Biochemistry 26*, 6664.

Cumming, D. A., Shah, R. N., Krepinsky, J. J., Grey, A. A., & Carver, J. P. (1987) *Biochemistry 26*, 6655.

Edge, C. J., Singh, U. C., Bazzo, R., Taylor, G. L., Dwek, R. A., & Rademacher, T. W. (1990) *Biochemistry 29*, 1971.

Forster, M., Mulloy, B., & Jones, C. (1989) *J. Mol. Graph. 7*, 196.

Homans, S. W. (1990) *Biochemistry 29*, 9110.

Homans, S. W., & Forster, M. (1992) *Glycobiology 2*, 143.

Homans, S. W., Dwek, R. A., Fernandes, D. L., & Rademacher, T. W. (1982) *FEBS Lett. 150*, 503.

Homans, S. W., Dwek, R. A., & Rademacher, T. W. (1987a) *Biochemistry 26*, 6553.

Homans, S. W., Dwek, R. A., & Rademacher, T. W. (1987b) *Biochemistry 26*, 6571.

Homans, S. W., Pastore, A., Dwek, R. A., & Rademacher, T. W. (1987c) *Biochemistry 26*, 6649.

Imberty, A., Tran, V., & Perez, S. (1989) *J. Comput. Chem. 11*, 205.

Kadkhodaei, M. M., Wu, H., & Brant, D. (1991) *Biopolymers 31*, 1581.

Kay, L. E., Torchia, D. A., & Bax, A. (1989) *Biochemistry 28*, 8972.

Lemieux, R. U., Bock, K., Delbaere, L. T. J., Koto, S., & Rao, V. S. (1980) *Can. J. Chem. 58*, 631.

Levy, G. C., Axelson, D. E., Schwartz, R., & Hochmann, J. (1978) *J. Am. Chem. Soc. 100*, 409.

Levy, R. M., Karplus, M., & McCammon, J. A. (1981) *J. Am. Chem. Soc. 103*, 994.

Lipari, G., & Szabo, A. (1982a) *J. Am. Chem. Soc. 104*, 4546.

Lipari, G., & Szabo, A. (1982b) *J. Am. Chem. Soc. 104*, 4559.

Macura, S., & Ernst, R. R. (1980) *Mol. Phys. 41*, 95.

McCain, D. C., & Markley, J. L. (1986) *J. Am. Chem. Soc. 108*, 4259.

Norwood, T. J., Boyd, J., Heritage, J. E., Soffe, N., & Campbell, I. D. (1990) *J. Magn. Reson. 87*, 488.

Paulsen, H., Peters, T., Sinnwell, V., Heume, M., & Meyer, B. (1986) *Carbohydr. Res. 156*, 87.

Peters, T., Brisson, J.-R., & Bundle, D. R. (1990) *Can. J. Chem. 68*, 979.

Poppe, L., Dabrowski, J., Leith, C.-W., Koike, K., & Ogawa, T. (1990) *Eur. J. Biochem. 189*, 313.

Sabesan, S., Bock, K., & Lemieux, R. U. (1984) *Can. J. Chem. 62*, 1034.

Scarsdale, J. N., Ram, P., Prestegard, J. H., & Yu, R. K. (1988) *J. Comput. Chem. 9*, 133.

Thogersen, H., Lemieux, R. U., Bock, K., & Meyer, B. (1982) *Can. J. Chem. 60*, 44.

Tran, V. H., & Brady, J. W. (1990) in *Computer Modeling of Carbohydrate Molecules* (French, A. D., & Brady, J. W., Eds.) ACS Symposium Series 430, American Chemical Society, Washington, D.C.

Tvaroska, I., Hricovini, M., & Petrakova, E. (1989) *Carbohydr. Res. 189*, 359.

Vliegenthart, J. F. G., Dorland, L., & van Halbeek, H. (1983) *Adv. Carbohydr. Chem. Biochem. 41*, 209.

Wormald, M. R., Edge, C. J., & Dwek, R. A. (1991) *Biochem. Biophys. Res. Commun. 180*, 1214.

Wuethrich, K. (1986) NMR of proteins and nucleic acids, Wiley, New York.

Yan, Z.-Y., & Bush, C. A. (1990) *Biopolymers 29*, 799.